



HAL
open science

Towards an industrial perspective for urea-to-hydrogen valorization by electro-oxidation on nickel(III): real effluents and pilot-scale proof of concept

Guillaume Hopsort, Elyes Piguet, Laure Latapie, Karine Groenen Serrano, Karine Loubière, Théodore Tzedakis

► To cite this version:

Guillaume Hopsort, Elyes Piguet, Laure Latapie, Karine Groenen Serrano, Karine Loubière, et al.. Towards an industrial perspective for urea-to-hydrogen valorization by electro-oxidation on nickel(III): real effluents and pilot-scale proof of concept. *Electrochimica Acta*, 2024, 479, pp.143886. 10.1016/j.electacta.2024.143886 . hal-04437925

HAL Id: hal-04437925

<https://ut3-toulouseinp.hal.science/hal-04437925>

Submitted on 5 Feb 2024

HAL is a multi-disciplinary open access archive for the deposit and dissemination of scientific research documents, whether they are published or not. The documents may come from teaching and research institutions in France or abroad, or from public or private research centers.

L'archive ouverte pluridisciplinaire **HAL**, est destinée au dépôt et à la diffusion de documents scientifiques de niveau recherche, publiés ou non, émanant des établissements d'enseignement et de recherche français ou étrangers, des laboratoires publics ou privés.



Distributed under a Creative Commons Attribution 4.0 International License



Towards an industrial perspective for urea-to-hydrogen valorization by electro-oxidation on nickel(III): Real effluents and pilot-scale proof of concept

Guillaume Hopsort^{*}, Elyes Piguet, Laure Latapie, Karine Groenen Serrano, Karine Loubière, Théodore Tzedakis^{*}

Laboratoire de Génie Chimique, Université de Toulouse, CNRS, INPT, UPS, Toulouse, France

ARTICLE INFO

Keywords:

Wastewater valorization
Urea electro-oxidation (UEO)
Hydrogen
Urine electrochemical treatment
Pilot-scale electrolyzer

ABSTRACT

This paper presents an investigation into urea-to-hydrogen valorization through electro-oxidation on nickel(III). The study has dual objectives: (i) to gain a better understanding of the effects of organic compounds (other than urea) in human urine on UEO and (ii) to upscale the process to pilot-scale. Initial voltammetric studies at lab-scale using real human urine showed that urea adsorption on nickel(III) sites, followed by its electro-oxidation, competes with molecules such as creatinine, histidine, and creatine. Notably, creatinine reduced the nickel(II) oxidation signal by up to 20 %, indicating its reaction precedence over urea. Additionally, the oxidation rate of urea by nickel(III) in urine exhibited a much lower partial order (0.1), as opposed to 0.3 in KOH solution, confirming the impact of competitive adsorption. Subsequently, UEO experiments were upscaled using a specially designed 1 L undivided tubular EC reactor operating in multi-pass mode. Potentiostatic electrolysis of a urea synthetic solution was conducted over 70 h, achieving nitrogen and carbon species mass balances of over 97 %—a milestone previously unreported at this scale. The study further examined the influence of operating parameters such as anode surface area, flow rate and applied potential on the EC process. This investigation underscored the impact of factor like reactor geometry, controlled potential and temperature on process efficiency. Parameters for optimal N₂ production, highest urea conversion rate, etc., were also defined. Finally, the electrolysis of human urine at pilot-scale unveiled new challenges distinct from those encountered with urea synthetic solutions.

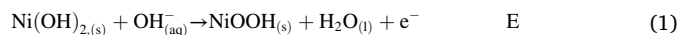
1. Introduction

To overcome both water pollution and energy challenges, urea contained in wastewater has been identified as a promising route [1]. Indeed, the rising freshwater contamination due to human activities (like the carbon industry, transportation, and the primary sector, including mining [2] and agriculture [3]) combined to the wastewater production, that is expected to surge by nearly 50 % by 2050 [4,5], have boosted the interest to consider wastewater as a significant source for pollutant valorization [6]. Among the contaminants, urea, primarily contained in human urine at around 0.33 mol L⁻¹, holds a substantial share of nitrogen (N) present in watercourses and thus offers a considerable source of nitrogen recovery [7]. Recognizing the potential for over half a century, researchers are delved into the electrochemical (EC) oxidation of urea with various purposes in mind, such as urine

degradation [11], H₂ production through electrolyzers [8], energy generation via urea fuel cells [9], and development of advanced electrode materials [10]. Among the key findings, one concerns the feasibility to achieve efficient urea electro-oxidation (UEO) using low-cost electrode materials in alkaline media, which clearly paves the way to potential industrial-scale implementation [11]. Notably, Ni-based anodes have demonstrated interesting electrocatalytic activity for the UEO process [12,13].

The UEO process has been long considered as an effective solution for the treatment of urea-laden effluents, with the dual advantage of generating eco-friendly by-products and reducing environmental impact according to the following indirect oxidation mechanism (EC^{*}).

At the anode:



^{*} Corresponding authors.

E-mail addresses: hopsort.guillaume@gmail.com (G. Hopsort), theodore.tzedakis@univ-tlse3.fr (T. Tzedakis).

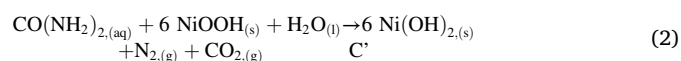
<https://doi.org/10.1016/j.electacta.2024.143886>

Received 2 November 2023; Received in revised form 27 December 2023; Accepted 26 January 2024

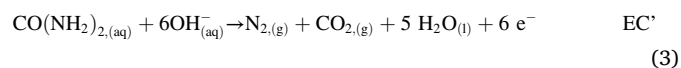
Available online 31 January 2024

0013-4686/© 2024 The Author(s). Published by Elsevier Ltd. This is an open access article under the CC BY license (<http://creativecommons.org/licenses/by/4.0/>).

Abbreviations		Greek letters	
<i>Latin letters</i>		α, β, γ	kinetic partial orders of urea, hydroxide, and NiOOH respectively (dimensionless)
E	potential (V)	<i>Acronyms</i>	
I	current (A)	CE	Counter Electrode
i	current density ($A\ m^{-2}$)	EC	ElectroChemical
i^*	limiting current density in absence of histidine during OH ⁻ oxidation ($A\ m^{-2}$)	FA	Formic Acid
k	reaction rate constant of r ($mol^{1-\alpha-\beta-\gamma}\ m^{3(\alpha+\beta)-2}\ s^{-1}$)	GC	Gas Chromatography
n_i	molar amount of the compound i (mol)	IC	Ion Chromatography
$n_{i,eq\ C}$	equivalent amount of the carbonaceous compound i during electrolysis (mol_C)	ICP-OES	Inductively Coupled Plasma - Optical Emission Spectrometry
$n_{i,eq\ C}^*$	initial equivalent amount of the identified carbonaceous species i (mol_C)	OA	Oxalic Acid
$n_{i,eq\ N}$	equivalent amount of the nitrogenous compound i during electrolysis (mol_N)	PMMA	Poly(methyl methacrylate)
$n_{i,eq\ N}^*$	initial equivalent amount of the identified nitrogenous species i (mol_N)	RDE	Rotating Disk Electrode
r	UEO kinetic law ($mol\ m_{electrode}^{-2}\ s^{-1}$)	RPM	Revolutions Per Minute
$S_{electrode}$	electrode surface (m^2)	STP	Standard Temperature and Pressure
		TOC	Total Organic Carbon
		UEO	Urea Electro-Oxidation
		WE	Working Electrode



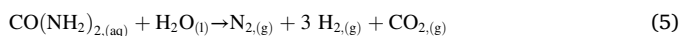
Net anodic reaction:



At the cathode:



Net cell reaction:



However, very recently, the formation of by-products (OCN^- , NO_2^- , NO_3^- , NH_3) other than N_2 and CO_2 (identified as CO_3^{2-} in alkaline medium) has been demonstrated. As posing major environmental concerns, some research efforts are now required, first to understand the related multi-pathway reaction mechanism and secondly to find solutions to orient the UEO process towards a full mineralization [14–17].

Moreover, the scaling of the UEO process to an industrial scale should rely on two factors: the use of affordable electrode materials and the generation of valuable hydrogen at the cathode. At present, the state-of-art on UEO focuses on lab-scale studies, and mainly on synthetic solutions. The proof-of-concept towards an industrial perspective should be thus refocused by accounting two issues: operating using real effluent (*i.e.*, human urine) and at pilot-scale, while maintaining the same performances than at lab-scale. So far, few studies have investigated the influence of the matrix on EC response (*i.e.*, of the urine chemical on the amplitude of the measured signal). Schranck et al. [18] performed cyclic voltammetry and ATR-FTIR spectroscopy to study the impact of urine-contained compounds on UEO using a $NiCo_2O_4$ catalyst on different substrates and synthetic urine solutions. They revealed that: (i) phosphate, creatinine (major organic compound after urea in human urine [19]) and proteins, were the major disruptors of electro-oxidation (creatinine could form deactivating complexes); and (ii) the weak binding of urea indicated its oxidation via an indirect electron transfer. Carpenter and Stuve [20] focused on the effect of creatinine during UEO and attributed the decrease in oxidation current during electrolysis of urea/creatinine solutions to the poisoning of electrode sites by creatinine or adsorbed fragments over long treatment periods. Our previous work [21] provided new highlights on real urine electrolyzes by

carrying out long-term experimentations on nickel massive electrode; in particular, the formation of two by-products (formic acid (FA) and oxalic acid (OA)) that were not present during the electrolysis of urea synthetic solutions was revealed. By monitoring the urea and creatinine concentrations over time, the competition between their oxidation could also be demonstrated. However, to date, any study on the effect of the actual matrix on EC behavior has been reported neither on a massive nickel electrode nor at larger scale using a Chemical Engineering framework.

This study is designed to address two specific challenges: (i) to enhance understanding of the matrix effect in the treatment of real human urine and its impact on UEO efficiency, and (ii) to demonstrate the feasibility of UEO at pilot-scale using both urea synthetic solutions and human urine. Accordingly, the results and discussion section is divided into two main parts. Section 3.1 will detail EC investigations of real urine at lab-scale through voltammetric analysis. It will first examine the effect of urine storage conditions, followed by an exploration of the system's EC response (namely, the nickel(II) oxidation current) to the spiking of primary urine compounds in different media (KOH, urea/KOH and urine/KOH in Section 3.1.2). This section will also report on the kinetics of the UEO reaction (Eq. (2)) in the presence of urine (Section 3.1.3). Section 3.2 will delve into pilot-scale experiments conducted in a 1 L EC reactor. For the first time, complete mass balances in both gaseous and aqueous phases will be established during the EC treatment of urea in synthetic solution (Section 3.2.1). This will be followed by a series of experiments to assess how operating parameters such as anode surface area, flow rate, and applied potential E influence process efficiency (Section 3.2.2). Finally, long-term electrolysis will be conducted in the pilot reactor with human urine, aiming to validate the overall process and identify any potential drawbacks.

2. Experimental

Two EC set-ups were considered in this work.

First, the same undivided three-electrode set-up (~50 mL) than the one described in a previous work [21] was used. It involved a nickel RDE working electrode (WE) (~3.14 mm²), a 316 L stainless counter electrode (CE) and a Hg/HgO/OH⁻ reference electrode.

Secondly, an undivided pilot-scale reactor and its environment (instrumentation, fluidics, etc.) were designed and built to treat urine by UEO. As illustrated in Fig. 1, it consisted in a vertical annular geometry with a volume of approximately 1 L. It was made of a nickel electrode

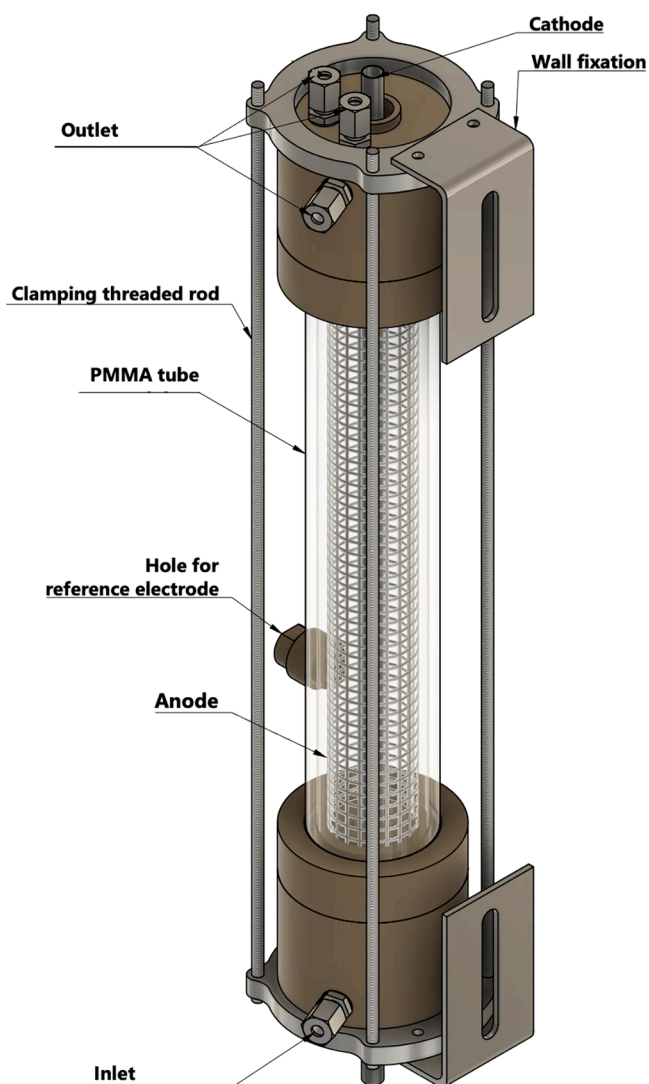


Fig. 1. Computer-aided design of pilot-scale EC reactor.

in grid form as anode (from 300 to 1100 cm²) and a 316 L stainless steel tube as cathode which was centered inside the anodic grid. The reaction medium thus flowed from the bottom to the top inside the annular section comprised between the external wall of the poly(methyl methacrylate) (PMMA) tube and the cathode. A Hg/HgO/OH⁻ electrode was used as the reference electrode. Note that, in this work, the potential values were systematically referred to the Hg/HgO/OH⁻ reference. As detailed in the Supporting Material (SM) – Section 1, this pilot-scale reactor operated in multi-pass closed mode by means of a thermo-regulated storage tank and a set of equipment.

For each set-up, the reaction medium was sampled at different times during the UEO process, and then analyzed by coupling ion chromatography (IC) to mass spectroscopy (liquid phase) and by gas chromatography (gas phase).

The experimental details (including the chemicals, characteristics of the EC cells at lab- and pilot-scales, and analytical methods) are given in the Supporting Material (SM) – Section 1.

3. Results and discussion

3.1. Electrochemical treatment of real urine at lab-scale

During long-term electrolyses, we have previously observed how the EC response of human urine was significantly different from the one

obtained with urea (such the formation of new by-products, FA and OA), which could be expected accounting for the complexity of the real matrix and the electro-activity of organic compounds [21]. In the present section, linear voltammetry experiments will be carried out to better understand the UEO mechanisms occurring with human urine. I-E curves will be plotted in order:

- (i) to highlight the phenomenon of urea hydrolysis in urine;
- (ii) to evaluate the influence of the matrix effect on the EC response;
- (iii) to determine the kinetic partial order of urea for the chemical reaction (Eq. (2)) between NiOOH and urea in the case of a real urine solution and comparing it with urea synthetic solution.

3.1.1. Electrochemical behavior of urine stabilized by alkalization

Fig. 2a shows typical linear voltametric curves obtained with a urea synthetic solution and a urine solution freshly excreted and alkalized at pH = 14 (equivalent to a KOH concentration of 1 mol L⁻¹).

Curves ② in Fig. 2a and ① in Fig. 2b correspond to the residual current obtained on nickel with KOH 1 mol L⁻¹ solution.

Two distinct regions can be observed on the curves ① and ② plotted in Fig. 2a and Fig. 2b respectively:

- (i) a first anodic signal occurs, exhibiting a plateau (~25 A m⁻²) in the potential range between -0.05 and 0.45 V vs. Hg/HgO/OH⁻. This wave is not observed in the case of urea synthetic solutions (curve ③ in Fig. 2a). After deep investigations, it can be attributed to the oxidation of uric acid (C₅H₄N₄O₃). Indeed, successive additions of uric acid quantities (from 1 to 4 mmol L⁻¹) allow to obtain curves in which the magnitude of this wave increases according to Eq. (6).

$$I_{E=0.4 \text{ V}} = 7.5 \times 10^{-6} + 4.7 \times 10^{-2} \times [\text{C}_5\text{H}_4\text{N}_4\text{O}_3] \text{ with } R^2 = 0.997 \quad (6)$$

where $I_{E=0.4 \text{ V}}$ is the current observed at 0.4 V (before Ni(II) oxidation, in A) and $[\text{C}_5\text{H}_4\text{N}_4\text{O}_3]$ is the uric acid concentration (mol L⁻¹).

- (i) a second oxidation signal exists between 0.45 and 0.55 V vs. Hg/HgO/OH⁻, which the magnitude (~50 A m⁻²) remains constant. This signal has been already observed with both KOH and urea synthetic solutions, and is attributed to the oxidation of Ni(II) to Ni(III). Note that (i) the potential of this wave is not modified in the case of “urine” matrix, and (ii) its magnitude in the case of urine (~50 A m⁻²) is lower compared to the one obtained with urea synthetic solutions (~280 A m⁻²), which means that the turnover number ([15], definition is reminded in Supporting Material – Section 1) is smaller.

A second series of experiments is carried out to investigate the long-term stability of urine samples and to study the kinetics of urea hydrolysis into the urine. For that, I-E curves are plotted over several days by implementing two situations for the same initial batch of urine:

- Case (i): a part of the urine sample is alkalized on the first day, and the I-E curves are plotted after various days’ storage;
- Case (ii): the other part of this urine sample is stored at room temperature, and periodically, an aliquot is undertaken, alkalized and analyzed.

Fig. 3 shows the I-E curves plotted with the urine solutions alkalized at different durations/ages (case (ii)). As shown in Fig. 3a, the first oxidation signal (-0.1 V vs. Hg/HgO/OH⁻) remains unaffected over time, while the anodic signal attributed to the Ni(II) oxidation decreases

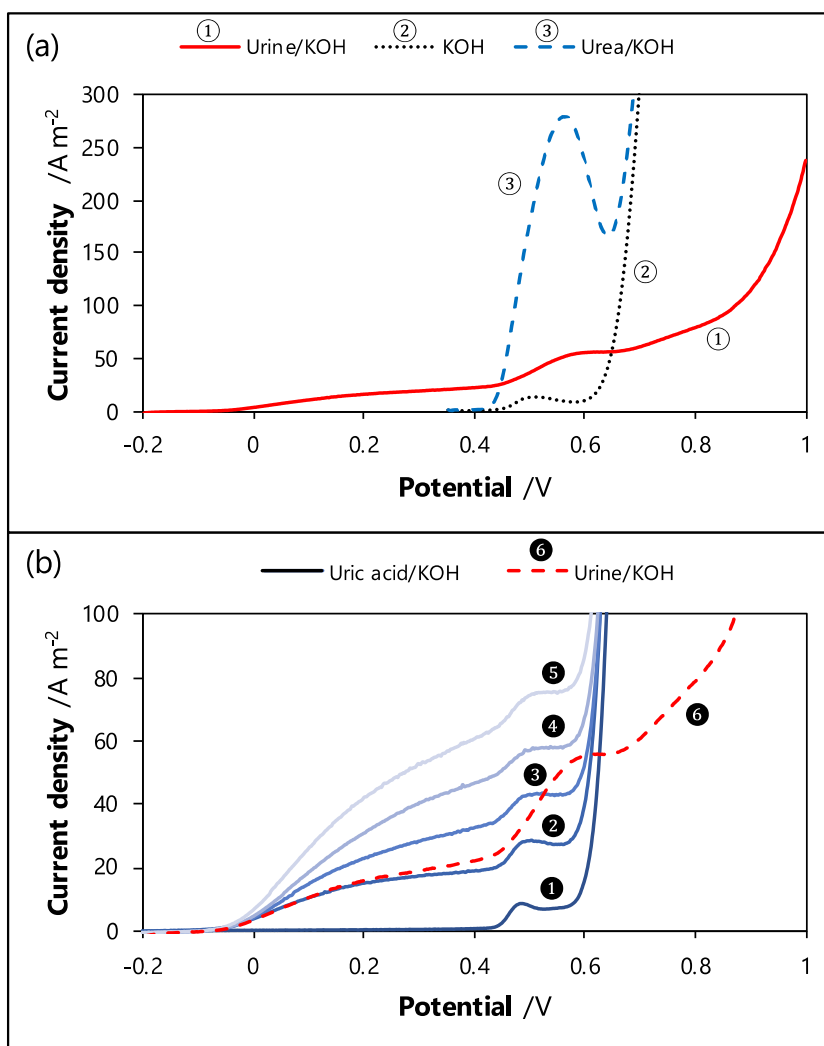


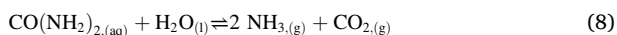
Fig. 2. (a) Linear voltammograms obtained with: a freshly excreted human urine immediately alkalinized with a KOH solution at 1 mol L^{-1} (solid line ①), a KOH solution at 1 mol L^{-1} (dotted line ②) and a urea solution at 0.33 mol L^{-1} alkalinized with KOH at 1 mol L^{-1} (dashed line ③). (b) Linear voltammograms obtained with: a freshly excreted human urine immediately alkalinized with a KOH solution at 1 mol L^{-1} (dashed line ⑥), and uric acid solutions (concentrations at ① 0 mmol L^{-1} ; ② 1 mmol L^{-1} ; ③ 2 mmol L^{-1} ; ④ 3 mmol L^{-1} and ⑤ 4 mmol L^{-1}) alkalinized with KOH at 1 mol L^{-1} (solid lines). All the curves were obtained on nickel RDE, at 1000 RPM and with a scan rate of 10 mV s^{-1} .

over time. Fig. 3b reports the temporal variation of the ratio of the net current at d -day (defined in Eq. (7)) to the initial net current.

$$I_{d\text{-day}}^{\text{net}} = I_{d\text{-day}}^{E=0.6\text{V}} - I_{d\text{-day}}^{E=0.4\text{V}} \quad (7)$$

From Fig. 3b, one can conclude that:

- (i) the Ni(II) oxidation current decreases with time in both cases. The urea is hydrolyzed, according to reaction presented in Eq. (8), and its concentration then decreases. As this Ni(II) oxidation is catalyzed by the presence of urea, the current magnitude logically falls down.



It should be noted that similar phenomena could occur with other electroactive species that could be absorbed at NiOOH sites and catalyze the electro-oxidation of Ni(II).

- (i) an equilibrium state is reached as the observed normalized current stabilizes after 2 days of urine storage ($\sim 75\%$ for case (i) and $\sim 60\%$ for case (ii)).
- (ii) the hydrolysis kinetics of urea (or even of the other adsorbed molecules) is slow down in alkaline conditions. Indeed, the decrease of the current is faster and stronger when urine is stored at neutral pH ($\sim -40\%$) than at $\text{pH} = 14$ ($\sim -25\%$). In alkaline conditions, the kinetic of urea degradation was found to be slowed down: for example, Wang et al. [22] showed that the hydrolysis of urea-N in the samples exposed to $\text{pH} = 12$ and $\text{pH} = 13$ resulted in a reduction of 27–35% and approximately 0.5%, respectively, when compared to the reference.

3.1.2. Voltammetric studies of various media spiked with key urinary elements

To deeply understand the matrix effect, various voltammetric studies will be carried out by spiking three different matrices: KOH, urea/KOH and urine/KOH. As a first approach, the solution's spiking is made on (i) the most concentrated compounds present in urine [19] and (ii) on the ones formed especially during the urine electrolysis (especially FA and OA). They are listed below:

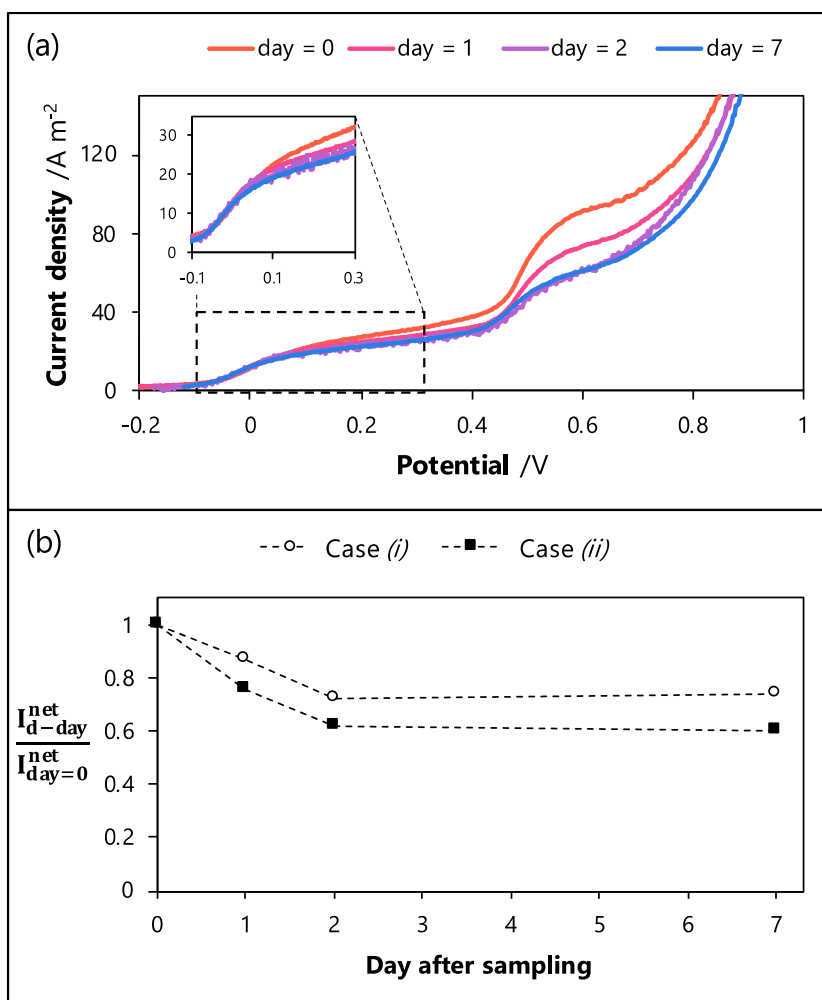


Fig. 3. Investigations of urine samples stability: (a) linear voltammetry of a urine solution at different days (up to 7 days) after excretion (alkalinized day-after-day, KOH 1 mol L⁻¹, 1000 RPM; 10 mV s⁻¹; case (ii)) and (b) temporal variation of the ratio of the net current at D-day to the initial net current (observed at 0.55 V vs. Hg/HgO/OH⁻) obtained from the urine solution alkalinized initially (case (i)) or day-after-day (case (ii)).

- organic molecules: creatinine (C₄H₇N₃O), hippuric acid (C₉H₉NO₃), creatine (C₄H₉N₃O₂), histidine (C₆H₉N₃O₂), oxalic acid (denoted OA, C₂H₂O₄) and formic acid (denoted FA, CH₂O₂);
- various ion compounds: phosphate (PO₄³⁻), sulfate (SO₄⁴⁻), chloride (Cl⁻) and ammonia (NH₃).

I-E curves, shown in the Supporting Material – Section 2, have been plotted under various operating conditions:

- an alkalinized solution ([KOH]= 1 mol L⁻¹);
- an alkalinized solution ([KOH]= 1 mol L⁻¹) containing urea at 0.33 mol L⁻¹;
- an alkalinized solution ([KOH]= 1 mol L⁻¹) containing urine in which urea is at 0.22 mol L⁻¹.

The obtained I-E curves exhibit some differences depending on the studied compound and matrix:

- hippuric acid, chloride, ammonia, sulfate and phosphate do not significantly affect the Ni(III)/Ni(II) signal, as the current remains constant whatever the added concentrations in KOH 1 mol L⁻¹ solution.
- creatinine, OA, creatinine and histidine seem to affect the electroactivity of the Ni(OH)₂ present at the surface of the electrode. Indeed, the magnitude of the corresponding current vary as a

function of the added concentration into the alkalinized solution. For example, at 50 mmol L⁻¹, it is 3.6 times (creatinine), 1.2 times (OA), 1.1 times (creatinine) and 1.1 times (histidine) higher compared to the initial current observed in unspiked solutions. This effect is less pronounced in the case of urea/KOH matrix (at 50 mmol L⁻¹; × 0.6, × 0.9, × 0.22 and × 0.2 respectively compared to the initial current observed in unspiked solutions).

- For urine/KOH matrix, the presence of OA, FA and creatine would not influence the Ni(II) signal. Conversely, doping this matrix by histidine, creatinine or even hippuric acid leads to decrease the current magnitude of the Ni(II) oxidation signal, and all the more for increasing added concentrations.

Fig. 4 summarizes these results by reporting the ratio of the net current of the Ni(II) oxidation signal for each spike to the net intensity before spiking.

Different conclusions can be drawn depending on the medium and on the concentrations (chosen to be close to physiological concentrations present in urine). They are discussed in the following sub-sections.

3.1.2.1. KOH medium. In this case, the oxidation of Ni(II) to Ni(III) takes place without catalysis and without continuous regeneration of Ni(II) by the chemical reaction with urea. An increase of the ratio $\frac{i_{\text{net}}^{\text{at } 0.55 \text{ V}}}{i_{\text{net}}^{\text{before spiking}}}$ means that the Ni(II) oxidation is exacerbated following two possible ways:

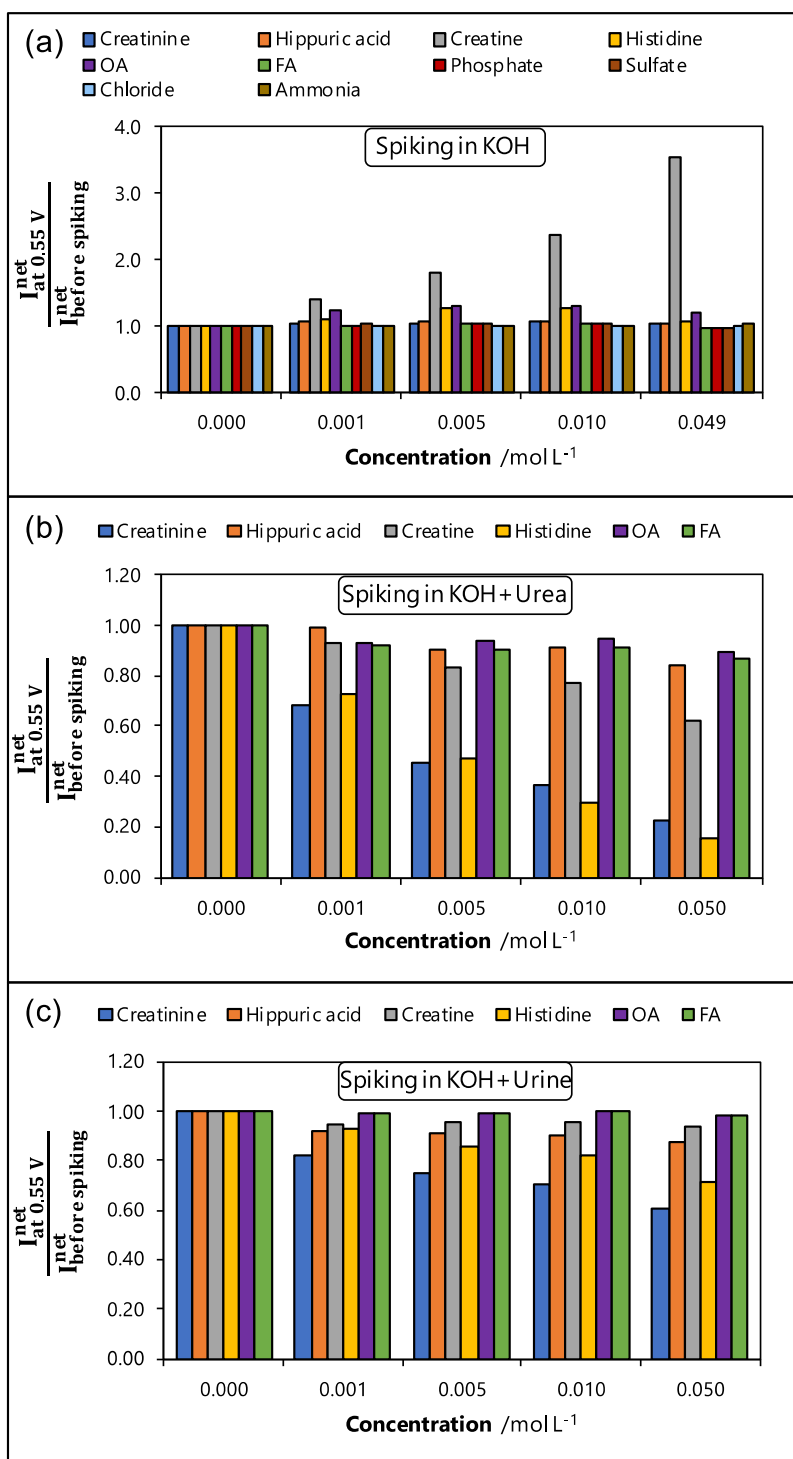
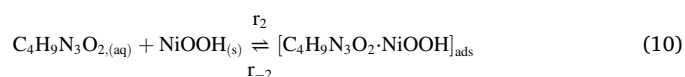
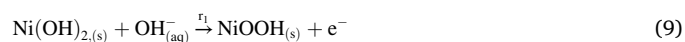


Fig. 4. Variation of the ratio of the net current of the Ni(II) oxidation signal for each spike to the net current before spiking as a function of the concentration of the spiked compound: (a) KOH, (b) urea/KOH and (c) urine/KOH media. The net currents are measured at 0.55 V.

- (i) by chemical reaction between NiOOH and the added species;
- (ii) by direct oxidation of the species added at the same potential than the oxidation of Ni(II).

From Fig. 4a, the main effect is observed with the creatine since the signal is multiplied by ~ 4 when adding 0.05 mol L^{-1} of creatine. The magnitude of the current oxidation of Ni(II) increases with the creatine concentration, but not linearly (Supporting Material – Section 2, Fig. S7). This behavior is similar to the one observed with urea. The

direct oxidation of creatine is thus excluded. By analogy, one can conclude that NiOOH oxidize creatine following the scheme presented in Eqs. (9)–(11) which involves the creatine adsorption on the NiOOH sites.





For creatine concentrations higher than 0.05 mol L^{-1} , the current stabilizes, meaning that the kinetic rate of the reaction (9), r_1 , is rapid and the kinetic rate of the forward direction of the reaction (10), r_2 , is dominant. The main limitation then comes from the reaction (11), r_3 .

To go further in the understanding of mechanism, additional investigation is required.

The effect of the concentrations of the other compounds appears minor, except probably for histidine ($\sim +0.03 \text{ V}$ when adding 0.05 mol L^{-1}) and creatinine ($\sim +0.02 \text{ V}$ when adding 0.05 mol L^{-1}) which seem to poison the electrode, as the Ni(II) oxidation potential increases over the concentration.

3.1.2.2. Urea/KOH matrix. In this medium, one should keep in mind that urea catalyzes the oxidation of Ni(II) to Ni(III) by chemical reaction. Fig. 4b clearly demonstrates the occurrence of a matrix effect. Indeed, compared with the KOH medium, the presence of organic molecules causes the magnitude of the Ni(II) oxidation signal to decrease. A competition for accessing to the Ni(III) sites is thus induced between urea and other molecules.

From Fig. 4b, creatinine, creatine and histidine are the main molecules affecting the current. The decrease is strongly pronounced in the case of histidine and creatinine. When considering the physiological concentrations into the urine, one can observe that:

- (i) creatine decreases the signal by 40 % (maximum physiological concentration of $2 \times 10^{-2} \text{ mol L}^{-1}$);
- (ii) creatinine decreases the signal by 80 % (maximum physiological concentration $3 \times 10^{-3} \text{ mol L}^{-1}$);
- (iii) histidine decreases the signal by 85 % (maximum physiological concentration $2 \times 10^{-3} \text{ mol L}^{-1}$).

This behavior is another indicator of the competitive adsorption of these molecules on Ni(III) sites against urea. Decreasing the amount of urea adsorbed leads to decrease the rate of the urea/Ni(III) reaction. Furthermore, these molecules can undergo reactions with Ni(III), and in such instances, they are selectively transformed, showing a preference over urea. The most unfavorable scenario occurs when these compounds adsorb onto the surface without interacting with Ni(III), resulting in the inhibition of urea oxidation.

The comparison of the current measured at $0.55 \text{ V vs. Hg/HgO/OH}^-$ observed after the maximum concentration spiking (all at 50 mmol L^{-1}) leads to the relation in Eq. (12).

$$I_{\text{Urea}} > I_{\text{FA}} > I_{\text{OA}} > I_{\text{Hippuric acid}} > I_{\text{Creatine}} > I_{\text{Creatinine}} \sim I_{\text{Histidine}} \quad (12)$$

Note that this current represents the oxidation of Ni(II) to Ni(III), followed by any potential oxidation of the preceding compounds, including urea, by NiOOH. In all cases, the observed current is lower than that of urea alone.

In conclusion, there is a competitive adsorption of these molecules, which induces a decrease in the current for the Ni(II)→Ni(III) reaction. At this stage, both chemical reactions (Ni(III)/urea and Ni(III)/other compounds) may occur, and the overall rate of Ni(III) reduction (*i.e.*, by urea and other compounds) decreases, depending on the number of available Ni(III) sites (*i.e.*, the respective adsorption affinity of urea and other compounds).

From this, one can deduce the order of the adsorption affinity of these adducts against the Ni(III) as follows:

$$\text{Creatinine} \sim \text{Histidine} > \text{Creatine} > \text{Hippuric acid} > \text{OA} > \text{FA} \quad (13)$$

3.1.2.3. Urine/KOH medium. The previously involved compounds have been also spiked in urine at $\text{pH} = 14$, even if they are already present in the solution. The results are presented in Fig. 4c. Compared to the previous medium (urea/KOH), the impact of these compounds on the Ni(II)

oxidation signal magnitude is lower: for example, for creatinine, the current is 30 % smaller while it is 80 % in the case of urea/KOH solution. As previously observed, only three compounds (creatinine, histidine and hippuric acid) exhibit a negative effect on the current that could be explained by an adsorption (competitive with urea) of the corresponding species onto the NiOOH sites and the subsequent poisoning of the electrode against, at the least urea oxidation.

3.1.2.4. Specific investigation on histidine. As shown in Fig. 4, histidine exhibits strong influence on both Ni(II) and solvent oxidations. Fig. 5a and 5b present the I-E curves obtained with various concentrations of histidine, in a potential scale going toward the anodic direction, until $2 \text{ V vs. Hg/HgO/OH}^-$. The goal is here to get a better understanding of the observed shift of the potential of both signals (*i.e.*, Ni(II) and OH^- oxidation reactions) to the anodic direction as a function of the increased concentration of histidine. The inset of Fig. 5b shows the Ni(II) oxidation signal.

The onset Ni(II) potential is slightly shifted to more anodic values (0.48 to $0.55 \text{ V vs. Hg/HgO/OH}^-$) when increasing histidine concentration, which confirms the adsorption of histidine on Ni(II). The resulting blocking of the nickel sites limits the access of OH^- to Ni(II). Besides, the amount of electrical charge of the Ni(II) oxidation signal decreases with histidine concentration (-30% between the signal before doping and with a doping at 0.05 mol L^{-1}).

For potentials higher than $0.6/0.7 \text{ V vs. Hg/HgO/OH}^-$, the oxidation of the hydroxyl ions occurs following the reaction (14).

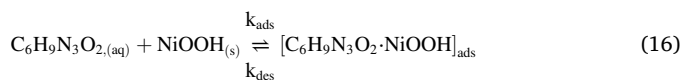


Curve in Fig. 5a (same as curve ① in Fig. 5b) is the signal obtained in the alkalized solution. For very high over-voltage ($E_{\text{anode}} > 2 \text{ V}$), the slope of the curve falls down (*i.e.*, to exhibit a OH^- diffusion-limited plateau at a magnitude of i^*). This means that at such potential range, the interfacial concentration of OH^- reaches low value and the new additional reaction occurring is the water oxidation described by the reaction (15). Note this also induces a decrease of the local pH.



In Fig. 5b, one can note that the corresponding part of the water oxidation does not appear in curve ① and ②, but it is clearly observable for curves ③ to ⑥. Curves ② to ⑥ have been obtained for various concentrations of histidine, from 1 to 50 mmol L^{-1} . They show that the current magnitude observed at the plateau decreases, thus confirming certain inhibition of the anode by the histidine against OH^- .

The next part expects to determine if the histidine adsorption could be modeled by the Langmuir model, assuming the following reaction (16).



As detailed in Supporting Material – Section 3, the following relationship can be established:

$$\frac{1}{|\Delta I|} = \frac{1}{I^*} + \frac{1}{K \times I^* \times [\text{Histidine}]} \quad (17)$$

where $|\Delta I|$ is the absolute value of the difference between the oxidation currents of hydroxide ions in presence and absence of histidine (A), I^* is the current in absence of histidine (A) and K is the equilibrium constant of the adsorption reaction (16) of histidine on nickel sites ($K = k_{\text{ads}}/k_{\text{des}}$, dimensionless).

Fig. 5c shows the variation of the inverse of $|\Delta I|$ as a function of the inverse of the histidine concentration (by assuming that the adsorbed quantity is negligible). A good agreement is found with Eq. (17) (correlation coefficient 0.99), validating the Langmuir-modeled of histidine adsorption onto nickel sites. The y-intercept of the straight line (equal to

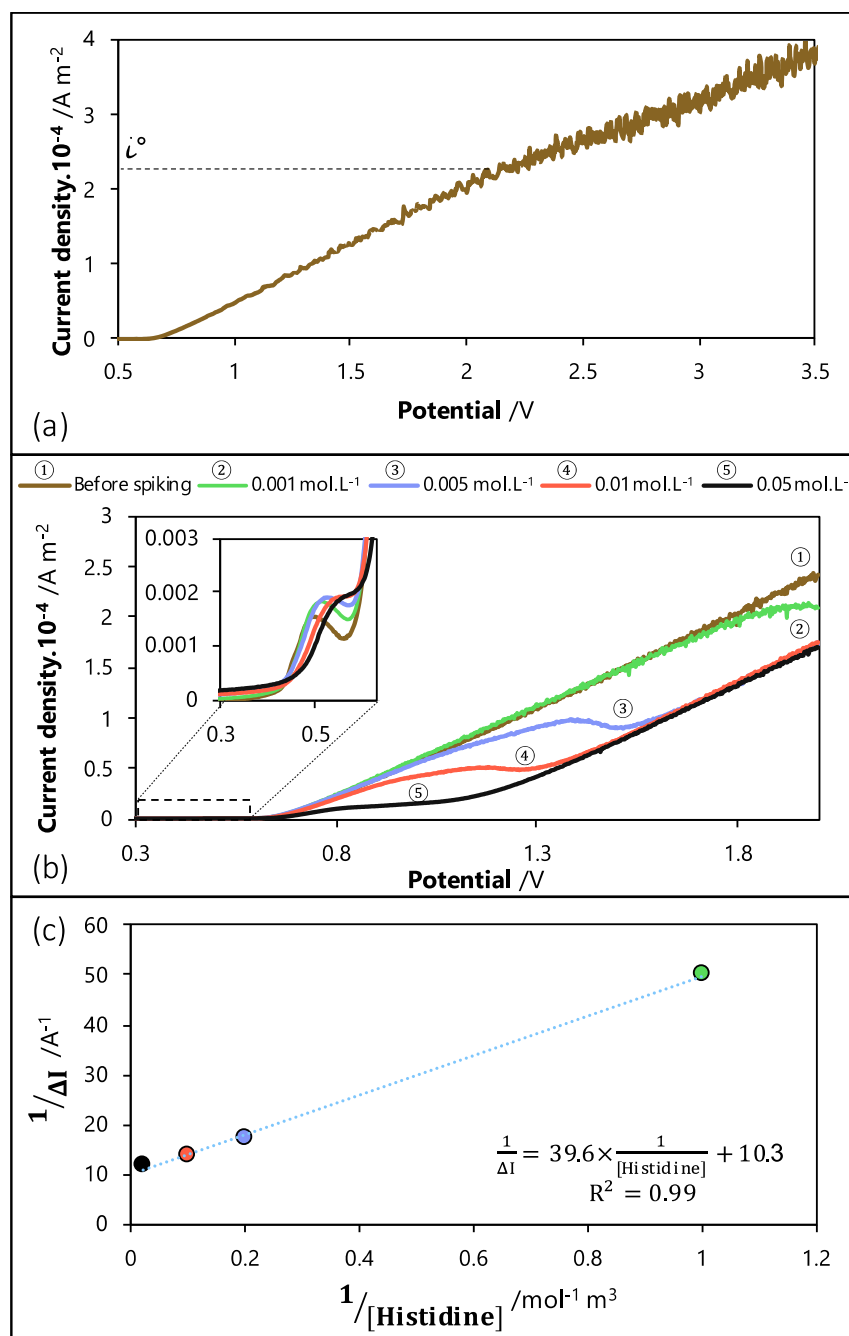


Fig. 5. Linear voltammograms obtained (a) with an alkalized solution ($[\text{KOH}] = 1 \text{ mol L}^{-1}$) and (b) when doping this alkalized solution with histidine for concentrations varying between 0.001 and 0.05 mol L^{-1} . (c) Determination of the affinity adsorption of histidine on nickel sites. All these results were obtained using the nickel RDE ($3.14 \times 10^{-6} \text{ m}^2$) at 6000 RPM and at a scan rate of 10 mV s^{-1} .

$1/I$, Eq. (17)) enables to determine the mass transfer coefficient of the hydroxide ions (in the case of 1 mol L^{-1} and an RDE anode surface area of 3.14 mm^2), as highlighted in Eq. (18). It is found equal to $8.4 \times 10^{-5} \text{ m s}^{-1}$.

$$k_{\text{OH}^-} = \frac{1}{y_{\text{intercept}} \times n_e \times \mathcal{F} \times [\text{OH}^-] \times S \times \frac{1}{1 - \alpha_{\text{OH}^-}}} \quad (18)$$

Assuming a diffusion coefficient of $5.3 \times 10^{-9} \text{ m}^2 \text{ s}^{-1}$ for hydroxide ions [23] and a transport number t_{OH^-} equal to 0.75 (as calculated in Supporting Material – Section 3), an external diffusion layer of $65 \mu\text{m}$ is obtained, which is in agreement with usual values. Having determined the k_{OH^-} coefficient, the histidine adsorption equilibrium constant, K ,

can be deduced and found equal to 0.22, meaning a relatively low affinity of histidine against nickel.

3.1.3. Impact of the matrix effect on UEO kinetic

In this last sub-section, the UEO kinetics will be investigated with a urine matrix expecting to determine the partial order of urea (for the chemical reaction urea/ OH^-/NiOOH , illustrated in reaction (2)) considering the following kinetic rate law:

$$r = k \times [\text{CO}(\text{NH}_2)_2]_{(t)}^\alpha \times [\text{OH}^-]_{(t)}^\beta \times (S_{\text{elec}})^\gamma \quad (19)$$

where k as the reaction rate constant ($\text{mol}^{1-(\alpha+\beta)} (\text{m}_{\text{elec}}^{-1})^{-(1+\gamma)} (\text{m}_{\text{bulk}}^3)^{\alpha+\beta-1} \text{ s}^{-1}$), S_{elec} the surface of the bare

nickel electrode (m_{elec}^2) and α , β , γ the partial orders of urea, hydroxide, and electrochemically generated nickel(III), respectively.

The methodology developed by [24] for urea/KOH medium has been here implemented for urine/KOH medium, so as to quantify the impact of the urine matrix on the UEO kinetics. The urea partial order is thus determined by plotting $I_{\text{net}}-E$ curves at a low scan rate (0.12 mV s^{-1}) for various concentrations of (added) urea into urine (see Fig. 6a and Eq. (20)), and the net current is calculated as:

$$\log\left(\frac{I_{\text{net,plateau}}^{\infty}}{I_{\text{net}}}\right) = \log\left(n \mathcal{F} \times k \times [\text{OH}^-]^{\beta} \times (S_{\text{electrode}})^{\gamma}\right) + \alpha \times \log\left([\text{CO}(\text{NH}_2)_2]\right) \quad (20)$$

where $I_{\text{net,plateau}}^{\infty}$ is the current corresponding to the plateau of the signal in steady state of the catalytic cycle between Ni(III) and urea (A) [24], n the number of exchanged electron (1, dimensionless) and \mathcal{F} the Faraday constant ($96,500 \text{ C mol}^{-1}$).

$$I_{\text{net}} = I_{E=0.57 \text{ V}} - I_{E=0.40 \text{ V}} \quad (21)$$

As demonstrated in [24], operating in this way (*i.e.*, at low potential scan rates) enables to minimize any limitation of the rate of the chemical reaction (Eq. (2)) by the oxidation of Ni(II) to Ni(III).

As shown in Fig. 6b, a straight line is obtained when plotting the logarithmic variation of the Ni(II) oxidation current against the urea

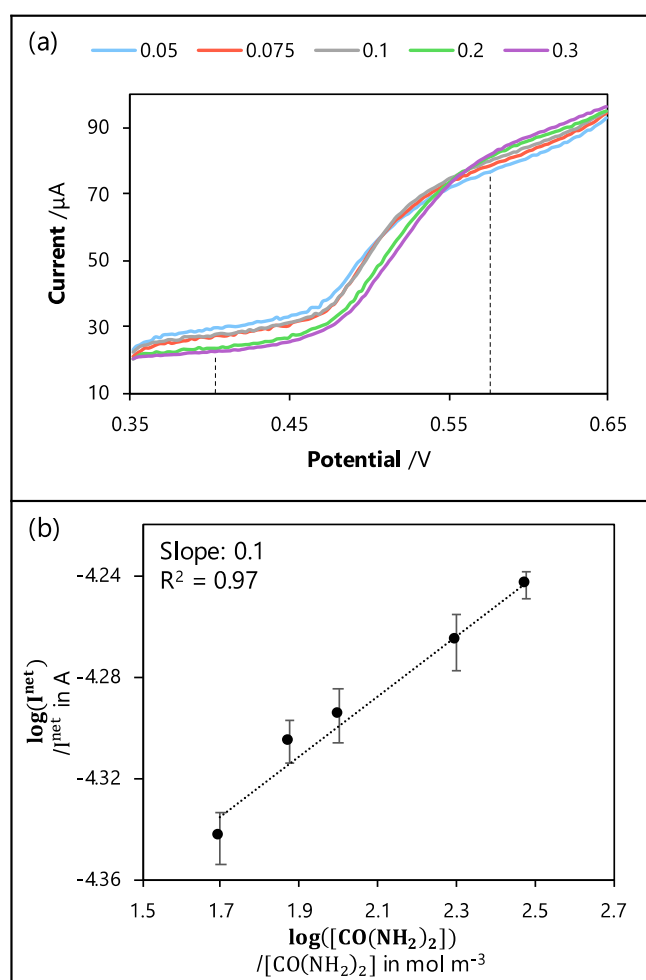


Fig. 6. Determination of the partial order of urea in urine/KOH medium: (a) I-E curves plotted for various concentrations of (added) urea, and (b) logarithmic variation of the Ni(II) oxidation net current against the urea (added) concentration. The potential scan rate was kept low (0.12 mV s^{-1}) for these experiments.

(added) concentration. As demonstrated in [24], the slope of this straight line is directly related to the value of the urea partial order, and the value is here found equal to 0.10 ± 0.05 . As a reminder, a value of 0.3 was obtained in a urea/KOH medium. The present low value indicates that the dependence of the Ni(II) oxidation current with respect to the urea concentration is poor, a direct consequence of (i) the adsorption competition effects, previously discussed and also (ii) the coupled indirect oxidation of both creatinine and urea.

3.2. UEO: from lab- to pilot-scale

This section is devoted to the extrapolation of the UEO process from lab-scale ($\sim 50 \text{ mL}$) to the pilot-scale ($\sim 1 \text{ L}$). The study will be composed of 3 parts aiming at:

- (i) implementing and discussing complete mass balances (in both liquid and gaseous phases) during the whole course of the UEO process in presence of urea synthetic solutions,
- (ii) studying the influence of operating parameters on the UEO performances in presence of urea synthetic solutions;
- (iii) establishing the proof of concept for pilot-scale electrolysis in presence of human urine solution.

3.2.1. Complete mass balances during urea electrolysis at pilot-scale

This section focuses on the performances obtained when a potentiostatic electrolysis of a urea solution is carried out. The potential is fixed at $0.55 \text{ V vs. Hg/HgO/OH}^-$, corresponding to the plateau obtained during Ni(II) oxidation coupled to the UEO. The results are plotted in Fig. 7.

Fig. 7a indicates the temporal variation of the current (black curve) and the volume of H_2 produced (red curve, in STP conditions). The current curve exponentially decreases over time. The initial value (0.25 A , equal to 3.41 A m^{-2}), relatively low, decreases 5 times after 70 h.

Fig. 7b introduces the time-dependent amount for the main analyzed compounds (urea, OCN^- , NO_2^- , NH_4^+ and N_2). One can first observe that the conversion of urea reaches 28 % after 70 h. Assuming that only urea is oxidized at the anode (to CO_2 and N_2 , *i.e.*, $6 e^-$), at the end of electrolysis, the magnitude of the current should be equal to 72 % of the initially observed current. That is not the case as it decreases 5 times (equivalent to 20 % of the initially observed one). This can be due to the fact that (i) a fraction of the dissolved H_2 is oxidized at the anode (and undergo subsequent oxidation) as the pilot-scale reactor presents an undivided configuration, and/or (ii) a deactivation of the nickel electrode occurs. The first assumption can be demonstrated by comparing the actual quantity produced $V_{\text{H}_2, \text{real}}$, determined by GC, and the quantity, $V_{\text{H}_2, \text{theoretical}}$, estimated from the electrical charge (considering that no H_2 oxidation is present) according to Eq. (22).

$$V_{\text{H}_2, \text{theoretical}} = \frac{\text{Charge } Q}{n_e \times \mathcal{F}} \times 22.4 \quad (22)$$

where n_e is the number of electrons exchanged (dimensionless, 2 in the case of $2 \text{ H}_2\text{O}_{(l)} + 2 e^- \rightarrow \text{H}_{2(g)} + 2 \text{ OH}_{(aq)}^-$).

At the end of electrolysis, Fig. 7a shows a 10 % deviation between the measured and theoretical volume of hydrogen, thus confirming the occurrence of either hydrogen oxidation at the anode or by-products reduction (such as NO_2^-) at the cathode (at the expense of H_2 production).

The cell voltage is indicated in the inset of Fig. 7a. The slight decrease in cell voltage (from 1.8 V down to 1.73 V) is ascribed to the decrease of both cathodic overvoltage and ohmic drop.

Fig. 7b points out that the degradation of urea primarily results in NH_3 (accounting for 13 mol.% at the end of the electrolysis, appearing as NH_4^+ in IC analysis). The formation of NH_3 has been discussed in numerous studies and its mechanistic aspects have been extensively

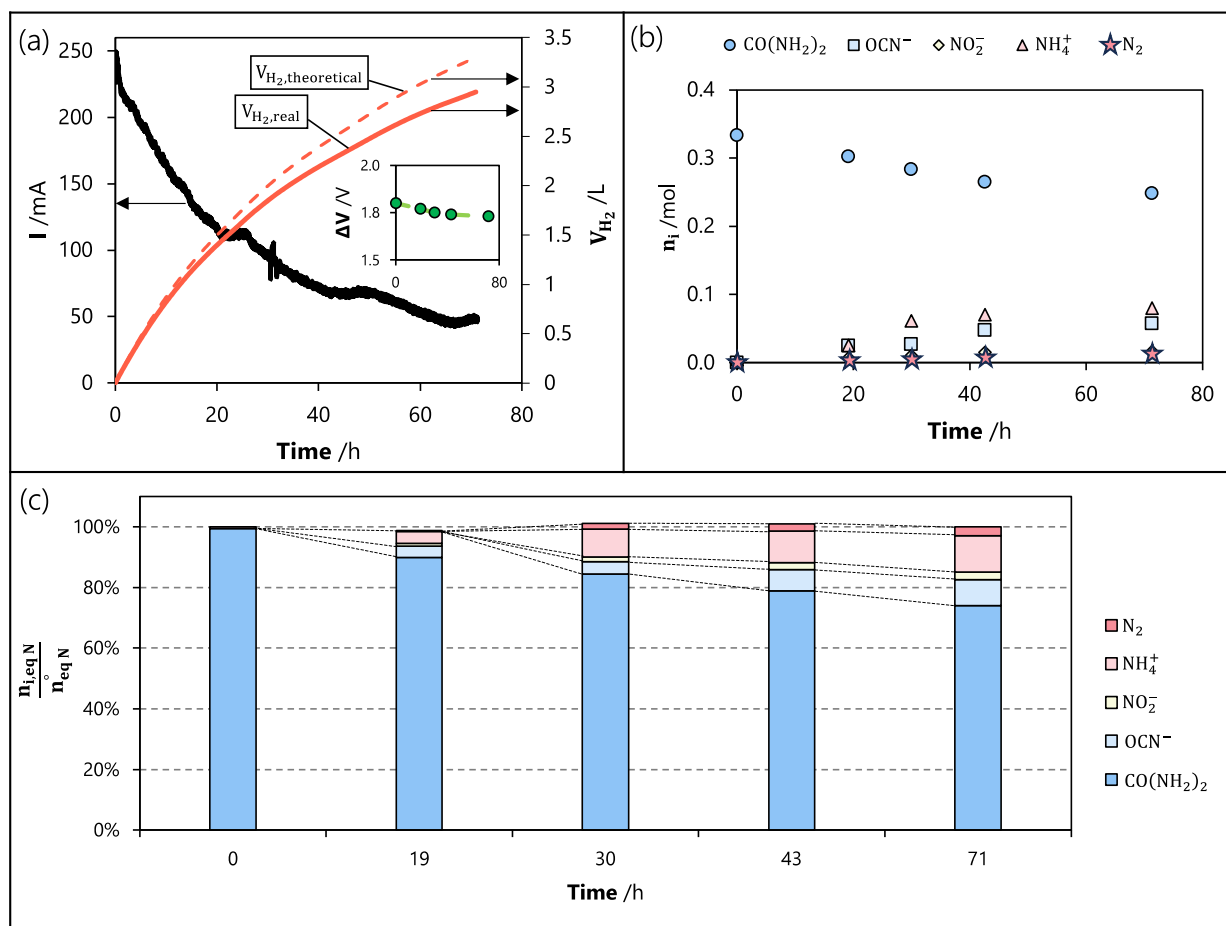


Fig. 7. Pilot-scale potentiostatic electrolysis (at 0.55 V vs. Hg/HgO/OH⁻) of a urea synthetic solution (0.33 mol L⁻¹) in alkaline medium (1 mol L⁻¹ KOH) with an anode surface of 734 cm², a volumetric flow rate of 29 L h⁻¹ ($Re = 155$): (a) current density and volume of electrogenerated H₂ (solid line: measured by GC, dashed line: theoretical volume), inset: cell voltage, (b) temporal profiles of molar quantity of the identified N-species, and (c) N-mass balance.

explored [24–27]. It is generally proposed that ammonia formation predominantly occurs through urea hydrolysis, potentially accelerated at locally acidic pH conditions due to the consumption of hydroxide ions at the anode. Cyanate is also significantly (~10 mol.%) present. Note that the N₂ gas and NO₂⁻ are present in smaller amounts (~5 mol.%).

Fig. 7c reports, for the first time, complete mass balances at pilot-scale of the N-species generated in both liquid and gas phases. Whatever the electrolysis time, the predominant (> 97 %) N-compounds created during electrolysis at this scale are OCN⁻, NO₂⁻, NH₃, and N₂. The mass balance of the C-species (specifically CO(NH₂)₂, OCN⁻, and CO₃²⁻) is reported in the Supporting Material – Section 4 and also corroborated (*i.e.*, exceeding 97 %). These findings are fully in agreement with the lab-scale results presented in a previous work [21].

3.2.2. Effect of key operating parameters on urea synthetic solution electrolyzes at pilot-scale

In this section, the impact on the UEO performances of three operating parameters will be investigated, namely:

- (i) the anode surface area;
- (ii) the flow rate of the urea solution into the undivided reactor;
- (iii) the applied potential.

3.2.2.1. Influence of the surface of the nickel grid anode. Fig. 8 shows the results of two potentiostatic electrolyzes (at 0.55 V vs. Hg/HgO/OH⁻) with two different anode surfaces: 734 cm² (2-cylinder revolutions of

nickel grid in the reactor, $S/V = 78 \text{ m}^{-1}$) and 1101 cm² (3-cylinder revolutions, $S/V = 117 \text{ m}^{-1}$).

The following conclusions can be drawn:

- (i) in Fig. 8a, when the geometrical surface is multiplied by 1.5, the initial current goes from 0.23 A (734 cm²) to 0.96 A (1101 cm²) and is therefore multiplied by approximately 4.2. It could be explained by (i) a stoichiometric ratio in favor of nickel(III) and (ii) the chemical kinetic rate law. This would be consistent with the partial order of nickel(III) determined in [24] (value of 5). Indeed, the chemical rate is not a linear function of the nickel site surface concentration, but proportional to S_{elec}^5 .
- (ii) Fig. 8b confirms that the variation of the volume of H₂ formed during electrolysis as a function of the electrical charge is not affected by the electrolysis surface. The time over which hydrogen is formed is shortened with a larger electrode surface area (3 L_{H₂} in 71 h vs. 3 L_{H₂} in 11 h).
- (iii) in Fig. 8b, the variation of the urea amount with the electrical charge is not affected when increasing the anode surface. However, the amount of oxidized urea is higher with larger electrode surface area (-0.08 mol_{urea} in 71 h vs. -0.14 mol_{urea} in 20 h).
- (iv) the nature of the by-products remains identical whatever the anode surface, as well as their proportions according to the electrical charge (the related data are reported in the Supporting Material – Section 5).

3.2.2.2. Influence of the flow rate. Fig. 9 shows both (i) the temporal

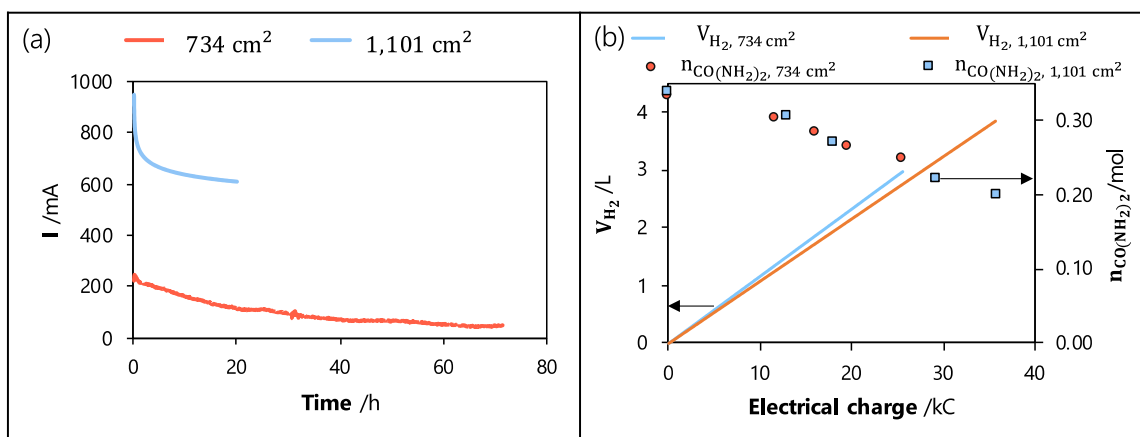


Fig. 8. Pilot-scale potentiostatic electrolyzes (at 0.55 V vs. Hg/HgO/OH⁻) of a urea synthetic solution (0.33 mol L⁻¹) in alkaline medium (1 mol L⁻¹ KOH) (29 L h⁻¹, undivided electrolyzer, 1 L) for two anodic surface areas (734 and 1101 cm²): (a) temporal profile of the current and (b) variation of the volume of the produced H₂ (continuous lines) and of the molar amount of unconverted urea (circles and squares) during electrolysis.

variation of the current magnitude and (ii) urea degradation measured during potentiostatic electrolyzes (at 0.55 V vs. Hg/HgO/OH⁻) carried out with two different flow rates: (i) 29 L h⁻¹ and (ii) 58 L h⁻¹.

When the flow rate is multiplied by 2, the current is increased by 20%. In both cases, the current decreases in a similar manner and their magnitudes are relatively close. This trend indicates a low mass transfer limitation, either from urea or OH⁻. The limitation to the process rate seems to be primarily attributed to the chemical reaction between Ni(III) and urea.

No change is observed between both flow rates concerning urea degradation (Fig. 9b) and the UEO by-products (Supporting Material – Section 6) against the electrical charge.

3.2.2.3. Influence of the applied potential. Fig. 10 shows the results of potentiostatic electrolyzes performed at three different applied potentials corresponding to Ni(II) oxidation (Fig. 2): (i) 0.45 V, (ii) 0.55 V and (iii) 0.65 V (vs. Hg/HgO/OH⁻).

The initial current magnitude increases as the applied potential increases (0.04 A at 0.45 V, 1.09 A at 0.55 V and 4.10 A at 0.65 V) as illustrated in Fig. 10a. All the currents decrease over time, translating the urea consumption, more rapidly at the higher potential value.

The urea degradation experimental profiles are shown in Fig. 10b. Increasing the applied potential causes, at identical electrolysis duration, an increase of the current magnitude, thus implying also an

increase of the urea conversion as indicated in the Table 1. However, no change is observed between both potential values concerning urea degradation (Fig. 10b) against the electrical charge.

The current decreases more rapidly than urea conversion, while, in theory, it is expected to decrease slowly as the urea oxidation generates various products, some of which may exhibit electroactivity at the nickel anode. This discrepancy indicates the existence of at least one competitive adsorption occurring on an intermediate product at the NiOOH surface. Increasing the applied potential appears to facilitate the oxidation of this intermediate, leading to the liberation of occupied Ni(III) sites.

The influence of applied potential on the molar amount of N-compounds is also investigated (note that in NO₂⁻ and N₂, the N-oxidation state is +III and 0, respectively). From Fig. 10c and 10d, one can compare the molar amount of nitrite produced with N₂. Increasing the applied potential tends to favor the NO₂⁻ formation. As presented in Table 2, the applied potential modifies the molar ratio of electro-generated N₂ and NO₂⁻. However, at 0.45 V vs. Hg/HgO/OH⁻, the N₂ obtained represents only 0.67 mol.% of the initial urea. The lower the potential, the more N₂ is formed from urea converted.

These results are similar to those obtained at lab-scale by Tatarchuk et al. [28] for both NO₂⁻ and N₂. Note that nitrate formation was also observed in their work at potentials higher than 0.77 V vs. Hg/HgO/OH⁻ (this range of potential values has not been investigated in this work).

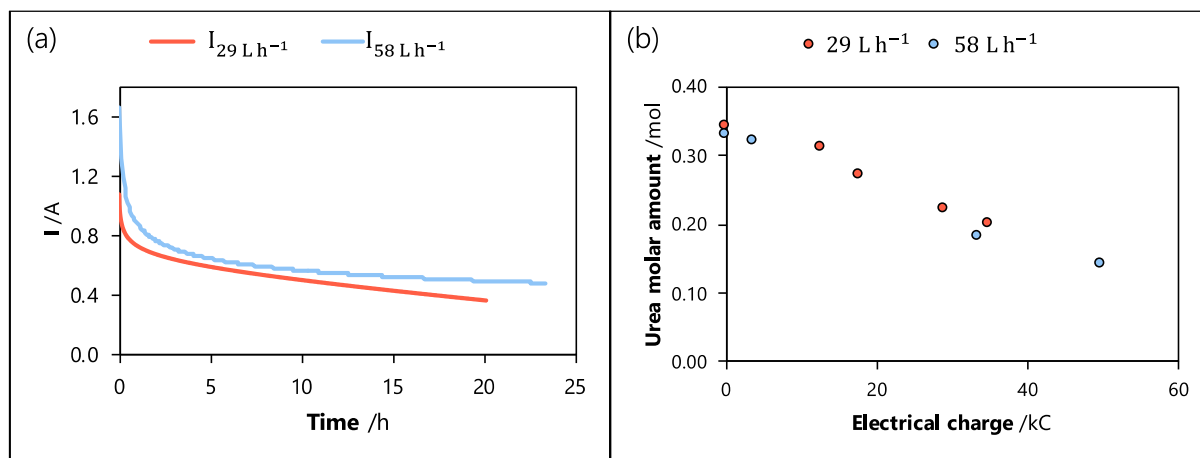


Fig. 9. Pilot-scale potentiostatic electrolyzes (at 0.55 V vs. Hg/HgO/OH⁻) of a urea synthetic solution (0.33 mol L⁻¹) in alkaline medium (1 mol L⁻¹ KOH; 1101 cm²; undivided electrolyzer; 1 L) for two different flow rates (29 and 58 L h⁻¹, corresponding to Re = 155 and 311): profiles of (a) the current and (b) the urea molar amount.

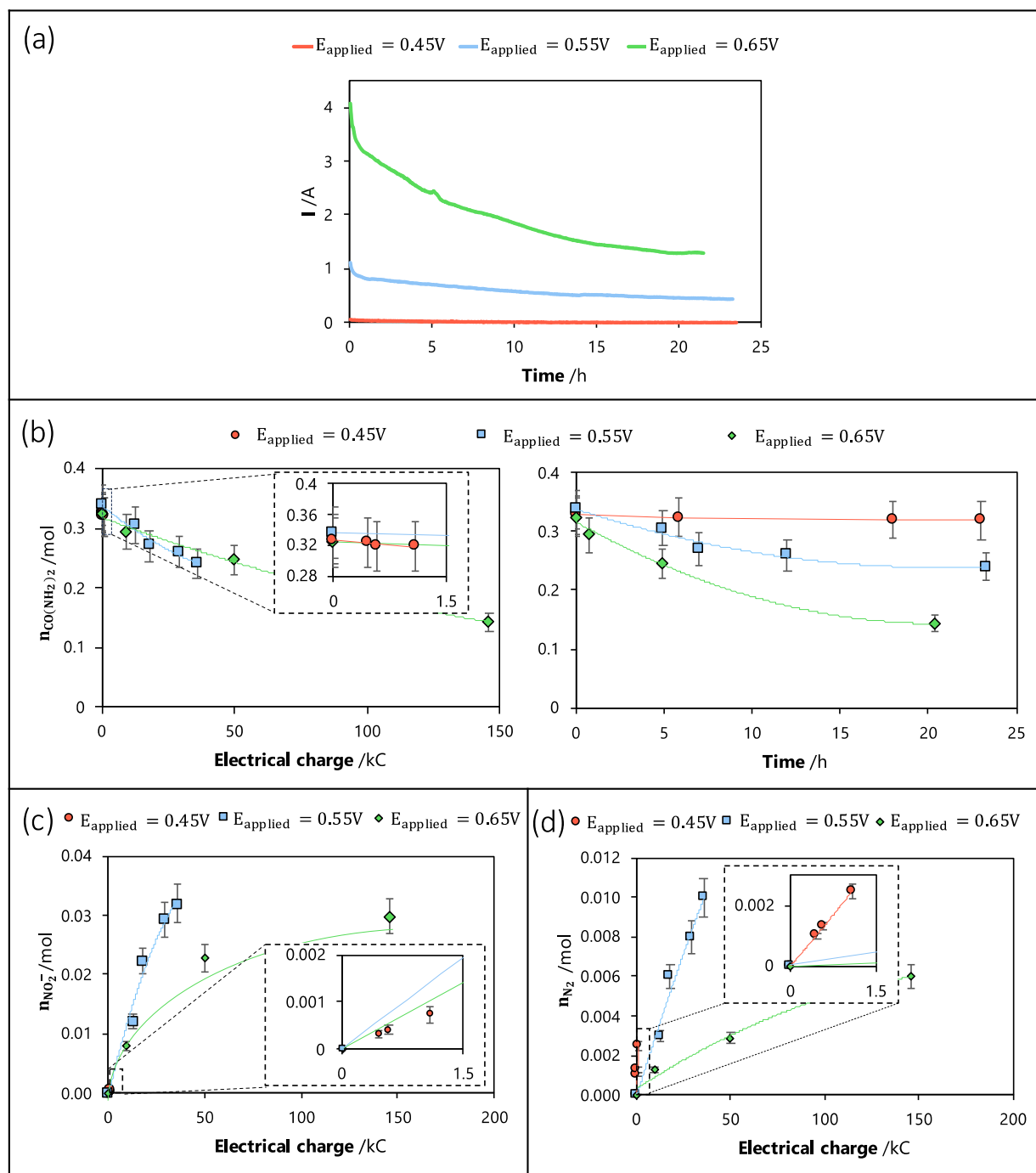


Fig. 10. Pilot-scale potentiostatic electrolyzes of a urea synthetic solution (0.33 mol L^{-1}) in alkaline medium ($1 \text{ mol L}^{-1} \text{ KOH}$, 1101 cm^2 , 58 L h^{-1} , undivided electrolyzer, 1 L) for three different applied potentials: (a) temporal profiles of the current, (b) variation of the urea molar amount with electrical charge and electrolysis time, (c) variation of the NO_2^- molar amount with electrical charge and (d) variation of the N_2 amount with electrical charge.

Table 1

Pilot-scale experiments: influence of the potential applied during electrolysis on urea conversion and current.

Applied potential E (V)	Electrolysis duration (h)	Electrical charge (kC)	Current decrease $\frac{i_{\text{initial}} - i_{\text{end}}}{i_{\text{initial}}}$ (% Fig. 10a)	Urea conversion (% Fig. 10b)
0.45	24	1.0	Non-significant	3
0.55	23	39.4	59	29
0.65	22	159.7	68	56

All these findings indicate that, to maximize the reactor's performance from an environmental point of view (*i.e.*, maximize N_2 and minimize nitrite), it is necessary to operate with high anode surface area and low volume of electrolyte (high specific surface area) at high flow rate. This enables to maximize the current, the urea conversion and the N_2 molar amount at the expense of the NO_2^- . The applied potential is identified as a key parameter as it allows to orientate N-compound formation mechanism.

3.2.3. Human urine electrolysis at pilot-scale

This last section presents the results obtained from pilot-scale

Table 2Pilot-scale experiments: Influence of the potential applied during electrolysis on NO_2^- and N_2 formations.

Applied potential (V)	Delivered charge (kC)	NO_2^-		N_2		$\frac{n_{\text{N}_2}}{n_{\text{NO}_2^-}}$ (dimensionless)
		Molar amount (mmol, Fig. 10c)	Amount corresponding to initial urea (i.e., 330 mmol,%)	Molar amount (mmol, Fig. 10d)	Amount corresponding to initial urea (i.e., 330 mmol,%)	
0.45	1	0.71	0.22	2.20	0.67	3.1
0.55		1.30	0.39	0.30	0.09	0.2
0.65		0.60	0.18	0.07	0.02	0.1

electrolysis of real urine solution.

Fig. 11 corresponds to a chronoamperometry electrolysis at 0.55 V vs. $\text{Hg}/\text{HgO}/\text{OH}^-$ on freshly excreted urine that has been alkalized. Note that the corresponding urea concentration in the urine was equal to 0.22 mol L^{-1} (corresponding to 30 % of the initial TOC).

Fig. 11a presents the temporal variation of the current; its initial value is relatively high (1.1 A) but drops drastically and immediately after polarization (decrease of 0.9 A in 1 h). After that, the current exhibits an exponential decrease and reaches 0.3 A after 24 h of electrolysis. Concerning the H_2 generation, the same evolution as the one for urea synthetic solution is evidenced by Fig. 11a (red curves). H_2 molecules (dissolved or gaseous) move from the cathode towards the anode and oxidize into water, thus causing a decrease of the faradic efficiencies of both urea and itself.

Fig. 11b reports the temporal variation of the TOC; a slight decrease ($\sim 3\%$) is observed after 24 h of electrolysis, although more than 30 kC is supplied to the system. This means that some oxidation of organic molecules occurs but without mineralization (i.e., the oxidation does not

generate $\text{CO}_2/\text{CO}_3^{2-}$). In addition, during the electrolysis, it has been observed that the solution colorizes into dark brown, thus indicating the oxidations of adducts into urine to some conjugated molecules (see Supporting Material – Section 7).

Fig. 11c shows the temporal variation of the molar amount of urea and creatinine, both initially present into urine in significant amounts. The initial concentration of creatinine ($9.5 \times 10^{-3} \text{ mol L}^{-1}$) is lower than the one of urea (0.22 mol L^{-1}). Both compounds are oxidized. However, the molar amount of creatinine decreases faster than urea. The final conversions reach 5 and 85 % for urea and creatinine respectively. Although, its lower concentration, creatinine first oxidizes and even appears to block/limit the urea oxidation. This behavior was also suggested at lab-scale [21] and thus clearly appears to be a serious drawback for the UEO process. However, if creatinine oxidation generated smaller products, then it is reasonable to imagine that, after creatinine oxidation, the urea oxidation would pursue. On another side, the creatinine oxidation products seem to present a certain passivating behavior against the Ni(II) oxidation, that could explain why the current

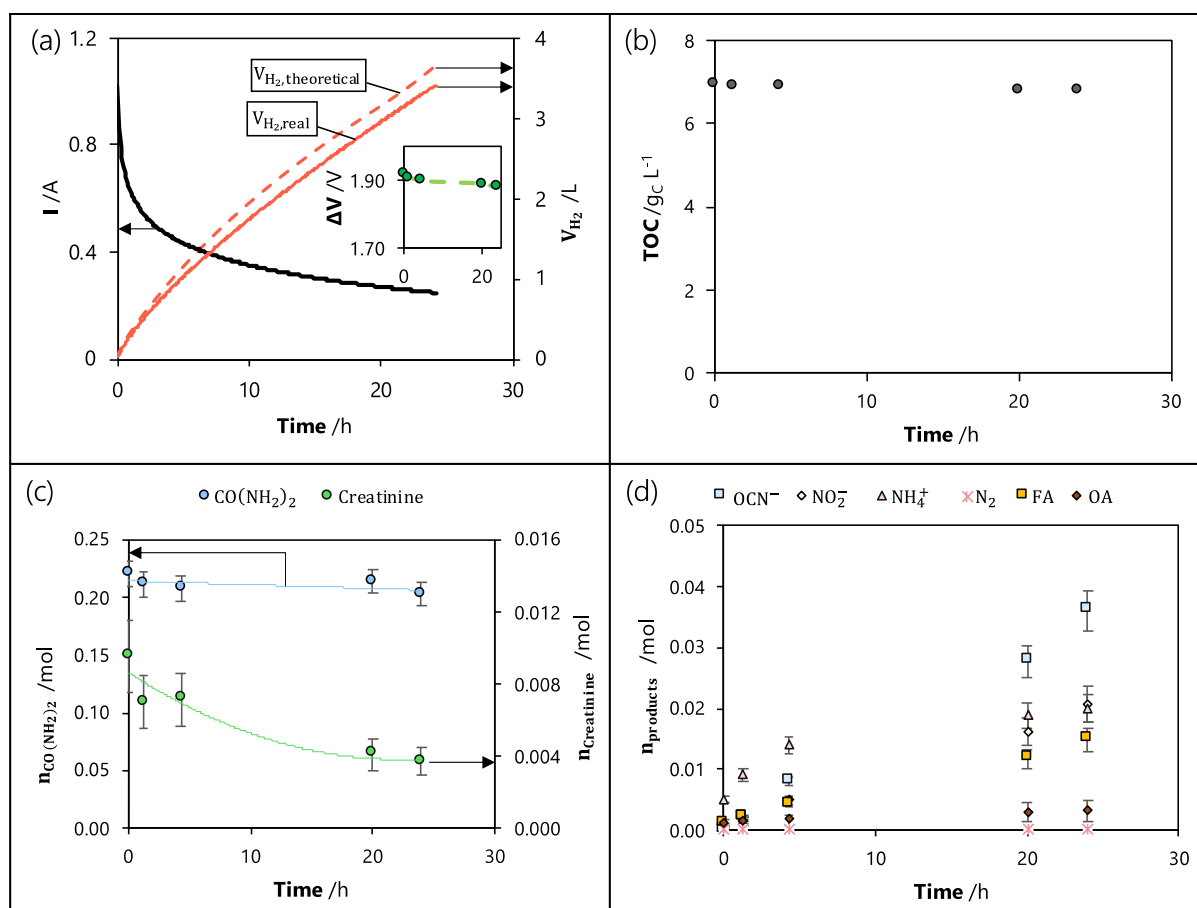


Fig. 11. Pilot-scale potentiostatic electrolysis (0.55 V vs. $\text{Hg}/\text{HgO}/\text{OH}^-$) of a human urine solution (urea concentration of 0.22 mol L^{-1}) in alkaline medium (1 mol L^{-1} KOH, 1101 cm^2 , 58 L h^{-1} , undivided electrolyzer, 1 L): temporal profiles of (a) the current and the formed H_2 amount (inset: cell voltage), (b) TOC, (c) urea and creatinine molar amount, (d) molar amount of identified generated products.

magnitude does not represent the quantity of the urea present in the solution (urea conversion does not exceeds 5 %).

In conclusion, (i) the substances present in urine, at the least creatinine, hinders UEO as already observed in lab-scale experiments, (ii) the stabilized current is low compared to the one expected when considering the residual concentrations of urea. This again validates the competition existing between urea and at the least creatinine (or histidine) for nickel sites.

Fig. 11d depicts the temporal profiles of the identified compound concentrations during potentiostatic electrolysis of human urine solution. OCN^- , NH_3 , NO_2^- , FA and OA are the main products. Their concentrations increase over time, suggesting oxidation of organic compounds. It has been demonstrated at a lab-scale that creatinine oxidizes into various by-products (e.g., OCN^- , NO_2^- , FA and OA [21]).

Lastly, despite the degradation of organic compounds caused by alkalization (~20 % of TOC at the time of alkalization and before electrolysis), the presence of surfactants or proteins in the treated urine is observed, as a significant layer of foam is formed inside the storage tank (Supporting Material – Section 7). Similarly, a brownish deposit can be seen on the reactor walls. The presence of nickel, possibly due to dissolution of the anode, remains always below $100 \mu\text{g.L}^{-1}$ (which is equal to the limit of detection, measured by ICP-OES after each electrolysis of the Section 3.2).

4. Conclusion

This study explored the intricacies of electrolyzing human urine, both at laboratory and pilot scales. The findings reveal the complex interactions within the chemical and electrochemical systems, particularly when dealing with this biological fluid.

At lab scale, voltammetric studies revealed the competitive adsorption and EC reactions of organic compounds—namely creatinine, histidine, and creatine—on nickel(III) sites, which in turn influenced the urea electro-oxidation. Notably, even at physiological concentrations, creatinine displayed a significant effect, by reducing the nickel(II) oxidation signal by approximately 20 %. This work demonstrates that the interaction among various organic compounds in human urine, which can influence the efficiency of the process, must be considered in the development of more efficient and selective EC treatment systems.

When scaled up to a pilot-scale 1 L reactor, trends not observed in lab-scale experiments emerged, including a significant decrease in current over time and a maximum urea degradation rate of 30 %. Interestingly, the nature of nitrogen and carbon compound by-products was identical and stable across the different anode surface areas and the flow rates, opening promising opportunities for optimizing process efficiency.

However, further research is warranted in several areas. First, investigating alternative materials (alloys, composites) and configurations for electrode design will be crucial [29], especially to address challenges like electrode partial deactivation by undesirable compounds in various types of urine. A deeper exploration of the influence of operating parameters, such as applied potential and galvanostatic operations, is necessary to maximize efficiency and selectivity in pilot-scale environments. Additionally, the practicality and scalability of this process in real-world settings pose challenges, underlining the necessity for pilot studies in actual wastewater treatment scenarios. Lastly, developing methods to recover and utilize valuable by-products, such as ammonia [30] and other nitrogen compounds [31–33], could offer significant benefits for agricultural or industrial applications.

In conclusion, this study not only sheds light on the EC properties of human urine but also opens avenues for innovative waste treatment technologies (particularly in resource-limited settings), and the recovery of valuable resources (circular economy), contributing to a more sustainable and efficient future by reducing the environmental footprint of waste management.

CRediT authorship contribution statement

Guillaume Hopsort: Conceptualization, Data curation, Formal analysis, Investigation, Validation, Visualization, Writing – original draft, Writing – review & editing. **Elyes Piguet:** Data curation, Formal analysis, Investigation, Validation. **Laure Latapie:** Resources. **Karine Groenen Serrano:** Conceptualization, Supervision, Writing – review & editing. **Karine Loubière:** Conceptualization, Supervision, Writing – review & editing. **Théodore Tzedakis:** Conceptualization, Funding acquisition, Project administration, Supervision, Writing – review & editing.

Declaration of competing interest

The authors declare that they have no known competing financial interests or personal relationships that could have appeared to influence the work reported in this paper.

Data availability

Data will be made available on request.

Acknowledgements

This work was supported by the French National Research Agency (proposals HYUREA ANR-19-CE04-0009).

Supplementary materials

Supplementary material associated with this article can be found, in the online version, at [doi:10.1016/j.electacta.2024.143886](https://doi.org/10.1016/j.electacta.2024.143886).

References

- [1] W. Sun, M. Zhang, J. Li, C. Peng, *ChemSusChem* 15 (21) (2022) e202201263, <https://doi.org/10.1002/cssc.202201263>.
- [2] M. Irfan, X. Liu, K. Hussain, S. Mushtaq, J. Cabrera, P. Zhang, *Environ. Sci. Pollut. Res.* 30 (28) (2021) 71585–71598, <https://doi.org/10.1007/s11356-021-13894-7>.
- [3] P.H. Gleick, H. Cooley, *Annu. Rev. Environ. Resour.* 46 (1) (2021) 319–348, <https://doi.org/10.1146/annurev-environ-012220-101319>.
- [4] A. Soares, *Environ. Sci. Ecotechnol.* 2 (2020) 100030, <https://doi.org/10.1016/j.ese.2020.100030>.
- [5] M. Qadir, P. Drechsel, B. Jiménez Cisneros, Y. Kim, A. Pramanik, P. Mehta, O. Olaniran, *Nat. Resour. Forum.* 44 (1) (2020) 40–51, <https://doi.org/10.1111/1477-8947.12187>.
- [6] M. Jeguirim, S. Jellali, *Water* 13 (4) (2021) 548, <https://doi.org/10.3390/w13040548>.
- [7] I. Kabdaşlı, O. Tünay, Ç. İşlek, E. Erdinç, S. Hüskalar, M.B. Tatlı, *Water Sci. Technol.* 53 (12) (2006) 305–312, <https://doi.org/10.2166/wst.2006.433>.
- [8] X. Sun, R. Ding, *Catal. Sci. Technol.* (2020), <https://doi.org/10.1039/C9CY02618E>.
- [9] E.T. Sayed, T. Eisa, H.O. Mohamed, M.A. Abdelkareem, A. Allagui, H. Alawadhi, K. J. Chae, *J. Power Sources.* 417 (2019) 159–175, <https://doi.org/10.1016/j.jpowsour.2018.12.024>.
- [10] K. Ke, G. Wang, D. Cao, G. Wang, *Electrocatalysis*, Springer International Publishing, Cham, 2020 (Ed: M. Shao).
- [11] E. Urbańczyk, M. Sowa, W. Simka, *J. Appl. Electrochem.* 46 (10) (2016) 1011–1029, <https://doi.org/10.1007/s10800-016-0993-6>.
- [12] R.K. Singh, K. Rajavelu, M. Montag, A. Schechter, *Energy Technol.* 9 (8) (2021) 2100017, <https://doi.org/10.1002/ente.202100017>.
- [13] Y. Ma, C. Ma, Y. Wang, K. Wang, *Catalysts* 12 (3) (2022) 337, <https://doi.org/10.3390/catal12030337>.
- [14] X. Wang, J. Li, Y. Duan, J. Li, H. Wang, X. Yang, M. Gong, *ChemCatChem* 14 (13) (2022) e202101906, <https://doi.org/10.1002/cctc.202101906>.
- [15] G. Hopsort, D.P.D. Carmo, L. Latapie, K. Loubière, K.G. Serrano, T. Tzedakis, *Electrochim. Acta* 442 (2023) 141898, <https://doi.org/10.1016/j.electacta.2023.141898>.
- [16] J. Li, J. Li, T. Liu, L. Chen, Y. Li, H. Wang, X. Chen, M. Gong, Z. Liu, X. Yang, *Angew. Chem. Int. Ed.* 60 (51) (2021) 26656–26662, <https://doi.org/10.1002/anie.202107886>.
- [17] W. Chen, L. Xu, X. Zhu, Y. Huang, W. Zhou, D. Wang, Y. Zhou, S. Du, Q. Li, C. Xie, et al., *Angew. Chem. Int. Ed.* 60 (13) (2021) 7297–7307, <https://doi.org/10.1002/anie.202015773>.

- [18] A. Schranck, R. Marks, E. Yates, K. Doudrick, *Environ. Sci. Technol.* 52 (15) (2018) 8638–8648, <https://doi.org/10.1021/acs.est.8b01743>.
- [19] S. Bouatra, F. Aziat, R. Mandal, A.C. Guo, M.R. Wilson, C. Knox, T.C. Bjorndahl, R. Krishnamurthy, F. Saleem, P. Liu, et al., *PLoS ONE* 8 (9) (2013) e73076, <https://doi.org/10.1371/journal.pone.0073076>.
- [20] K. Carpenter, E.M. Stuve, *J. Appl. Electrochem.* 51 (6) (2021) 945–957, <https://doi.org/10.1007/s10800-021-01545-1>.
- [21] G. Hopsort, L. Latapie, K. Groenen Serrano, K. Loubière, T. Tzedakis, *J. Electrochem. Soc.* 170 (9) (2023) 093507, <https://doi.org/10.1149/1945-7111/acf87e>.
- [22] W. Yang, J. Li, X. Yang, *Front. Sustain.* 2 (2021) 710739, <https://doi.org/10.3389/frsus.2021.710739>.
- [23] E. Samson, J. Marchand, K.A. Snyder, *Mater. Struct.* 36 (3) (2003) 156–165, <https://doi.org/10.1007/BF02479554>.
- [24] G. Hopsort, L. Latapie, K. Groenen Serrano, K. Loubière, T. Tzedakis, *AIChE J.* 69 (9) (2023) e18113, <https://doi.org/10.1002/aic.18113>.
- [25] F. Lu, G.G. Botte, *Electrochim. Acta* 246 (2017) 564–571, <https://doi.org/10.1016/j.electacta.2017.06.055>.
- [26] S. Akkari, V. Vivier, C.M. Sánchez-Sánchez, *Electrochim. Acta* 474 (2024) 143526, <https://doi.org/10.1016/j.electacta.2023.143526>.
- [27] F. Lu, G.G. Botte, *ECS Electrochem. Lett.* 4 (10) (2015) E5–E7, <https://doi.org/10.1149/2.0041510eel>.
- [28] S.W. Tatarchuk, J.J. Medvedev, F. Li, Y. Tobolovskaya, A. Klinkova, *Angew. Chem. Int. Ed.* 61 (39) (2022) e202209839, <https://doi.org/10.1002/anie.202209839>.
- [29] Q. Zhang, F. Md. Kazim, S. Ma, K. Qu, M. Li, Y. Wang, H. Hu, W. Cai, Z. Yang, *Appl. Catal. B Environ.* 280 (2021) 119436, <https://doi.org/10.1016/j.apcatb.2020.119436>.
- [30] C. Shin, A. Szczuka, M.J. Liu, L. Mendoza, R. Jiang, S.H. Tilmans, W.A. Tarpeh, W. A. Mitch, C.S. Criddle, *Environ. Sci. Technol.* 56 (12) (2022) 8712–8721, <https://doi.org/10.1021/acs.est.1c07992>.
- [31] A. Beckinghausen, M. Odlare, E. Thorin, S. Schwede, *Appl. Energy.* 263 (2020) 114616, <https://doi.org/10.1016/j.apenergy.2020.114616>.
- [32] Y. Zhou, Y. Zhu, J. Zhu, C. Li, G. Chen, *Int. J. Environ. Res. Public Health.* 20 (4) (2023) 3429, <https://doi.org/10.3390/ijerph20043429>.
- [33] Y. Qin, K. Wang, Z. Zhou, S. Yu, L. Wang, Q. Xia, X. Zhao, C. Zhou, J. Ye, Z. Wu, *Chem. Eng. J.* 455 (2023) 140337, <https://doi.org/10.1016/j.cej.2022.140337>.